

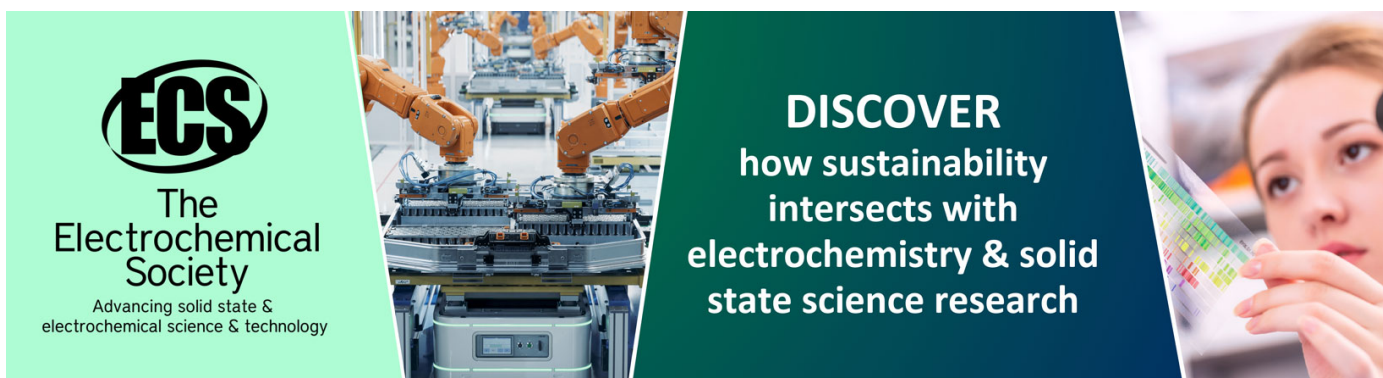
## Analysis on the uniformly loaded rectangular cross-section cantilever by a modified load–deflection model

To cite this article: Shang-Hsi Tsai *et al* 2009 *J. Phys. D: Appl. Phys.* **42** 045505

View the [article online](#) for updates and enhancements.

### You may also like

- [A design methodology based on full dynamic model for magnetorheological energy absorber equipped with disc springs](#)  
Mengjie Shou, Changrong Liao, Honghui Zhang *et al.*
- [A series solution approach to an analytical load-deflection relation for the measurement of mechanical properties of thin films](#)  
C T Loy, S C Pradhan, T Y Ng *et al.*
- [Rapid fabrication and characterization of MEMS Parylene C bellows for large deflection applications](#)  
H M Gensler and E Meng



**ECS**  
The  
Electrochemical  
Society  
Advancing solid state &  
electrochemical science & technology

**DISCOVER**  
how sustainability  
intersects with  
electrochemistry & solid  
state science research

# Analysis on the uniformly loaded rectangular cross-section cantilever by a modified load–deflection model

Shang-Hsi Tsai, Yeng-Tseng Wang and Heng-Chuan Kan

National Center for High-Performance Computing, No. 28, Nan-Ke 3rd Road, Hsin-Shi, Tainan County, 74147, Taiwan

E-mail: [shangsi@ntu.edu.tw](mailto:shangsi@ntu.edu.tw)

Received 18 November 2008, in final form 23 December 2008

Published 21 January 2009

Online at [stacks.iop.org/JPhysD/42/045505](http://stacks.iop.org/JPhysD/42/045505)

## Abstract

The load–deflection relationship of the uniformly loaded rectangular cross-section cantilever is analysed by a modified mechanical model, which exhibits its conformity to the physical situation by considering both the tangential and normal surface stresses. The analytical solution of the modelling equation is solved and presented in terms of the first and the second kinds of the Airy functions in association with Scorer's function. The resultant deflection profile contains an inflection point due to the restoring bending moment contributed by the critical surface loadings. The relationships of the tip deflection and the loading scenario are investigated, which reveal the fact that various loading scenarios can result in different deflection profiles, albeit with the same tip deflection. A numerical algorithm is given in the appendix to solve the loading scenario, by which the surface loadings can formally be determined for the designated applications for the devices utilizing the cantilever structure.

## 1. Introduction

Cantilever-based devices have been exploited as sensors [1–9] in the last decade by detecting the deflection and calculating the surface stresses induced by the interaction between the cantilever and the surroundings. For most of the applications, the classical Stoney's equation and its modifications are employed for the designated purposes by detecting the tip deflection and analysing the corresponding surface loadings [3, 4, 7–20]. The feature of the Stoney-type models is that the cantilever is deflected by nothing but the loadings parallel to the surface, concentrated or distributed [11, 21], and the resultant deflection profile is a monotonic increasing or decreasing function without being inflected. However, interactions in the normal direction should be taken into account, by which the restoring bending moment can be initiated from any kind of disturbances in practical situations, such as, the gravity of the overlying objects, the differential pressure from the ambient medium, and the immobilization of the analyte molecules binding on the cantilever surfaces. Otherwise, any minute repulsive perturbation will detach everything from the cantilever surface and eventually fail the designated purpose since nothing is detected by the device.

Another issue should be considered. From the experimental perspective, the quality and the quantity as well of a cantilever-based measurement are dependent on the parameters of the underlying mechanical model employed to characterize the deflection. For the Stoney-type model and the model studied in this work, the deflection is characterized by two kinds of parameters: the exerted surface loadings and the location of the neutral surface. As mentioned above, the loading scenario is analysed by the tip deflection for most applications. However, such a measurement may lead to ambiguity since different loading scenarios can bend the cantilever with the same tip deflection, especially for the devices deflected by distributed surface loadings. Therefore, measurements in addition to the tip deflection are required to correctly determine the loading scenario.

This paper investigates the load–deflection relationship of the rectangular cross-section cantilever by a modified mechanical model, which takes both the tangential and the normal surface stresses into consideration. The resultant deflection profile contains an inflection point due to the intrinsic restoring bending moment contributed by the critical surface loadings. In section 2, the modelling equation is developed by the principle of virtual work (PVW) [21–23] and

is presented as a non-dimensional inhomogeneous fourth-order linear ordinary differential equation with boundary conditions. The deflection and curvature profiles are analytically solved and expressed in terms of the first and second kinds of the Airy functions,  $Ai(X)$  and  $Bi(X)$ , in association with Scorer's function  $Gi(X)$  [24–26]. The series solution is provided in the appendix for [27]. In section 3, the critical loading scenario and the inflection point for the deflection profile are solved from the intrinsic bending moment. The relationships of the tip deflection and the loading scenarios are analysed and demonstrated by numerical examples, which reveal the fact that various loading scenarios can achieve the same tip deflection albeit with different deflection profiles. A numerical algorithm assuming that the whole deflection profile is measurable is given in the appendix to solve the loading scenario by the analytical solution developed in section 2. It is to be emphasized that to the authors' knowledge the whole cantilever deflection profile is yet unavailable. Therefore, the algorithm is just proposed without experimental verification.

## 2. Mechanical model and the analytical solution

This section develops the modified model for the deflection of the rectangular cross-section cantilever originally proposed by Zhang *et al* [21]. The analytical solution to the modelling equation is derived and is used to investigate the load–deflection relationship in the following section.

### 2.1. Development of the mechanical model

As illustrated in figure 1, the rectangular cantilever is of length  $L$ , width  $w$  and thickness  $t$  and is loaded on the top surface by a uniformly distributed normal surface stress  $\sigma_n$  and tangential surface stress  $\sigma_t$ , as shown in figure 1. The dimension of the exerted surface stresses is force per unit area. The downward normal and the tangential tensile surface stresses and the convex bending moment are designated as positive for sign convention. The modelling differential equation of the deflection and the corresponding boundary conditions at equilibrium can be derived by PVW [21–23] as follows. The elastic strain energy  $V$  stored in the deflected cantilever beam is given as

$$V = \int_0^L \frac{E^* I_N}{2} \left( \frac{d^2 y}{dx^2} \right)^2 dx,$$

where  $E^* = E/(1 - \mu)$  is the biaxial modulus [15],  $E$  and  $\mu$  are Young's modulus and Poisson's ratio, respectively and  $I_N$  is the area moment of inertia with respect to the neutral surface at the depth  $t_N$ . The external work done on the stressed beam can be presented as

$$W = - \int_0^L \frac{\sigma_t w}{2} (L - x) \left( \frac{dy}{dx} \right)^2 dx + \int_0^L \left[ \sigma_t t_N w (L - x) + \frac{\sigma_n w}{2} (L - x)^2 \right] \left( \frac{d^2 y}{dx^2} \right) dx.$$

By applying PVW,  $\delta(V - W) = 0$ , the differential equation and the boundary conditions characterizing the load–deflection

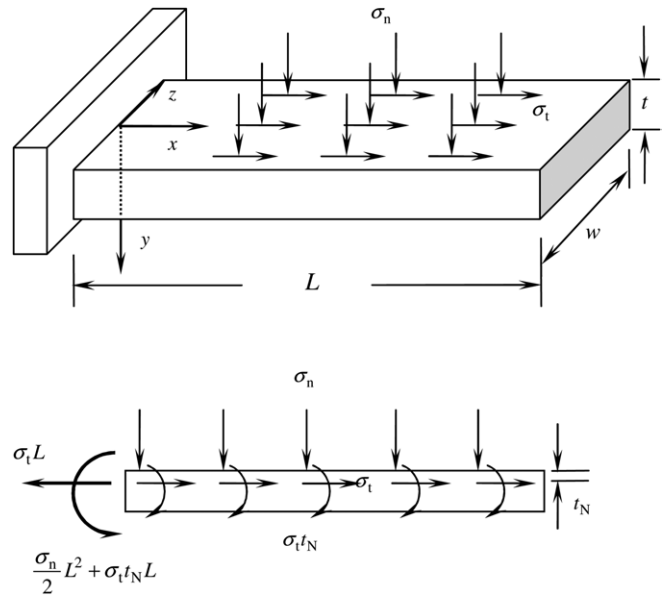


**Figure 1.** Schematic diagram of the cantilever beam dimensions, coordinates and the loading scenarios of the present model [21, 24, 27].

relationship are derived as

$$E^* I_N \frac{d^4 y}{dx^4} - \sigma_t w (L - x) \frac{d^2 y}{dx^2} + \sigma_t w \frac{dy}{dx} = \sigma_n w$$

for  $0 \leq x \leq L$ , (1)

$$y(0) = \frac{dy}{dx}(0) = \frac{d^2 y}{dx^2}(L) = E^* I_N \frac{d^3 y}{dx^3}(L) + \sigma_t t_N w = 0. \quad (2)$$

Equation (1) and boundary conditions (2) can be non-dimensionalized as an inhomogeneous fourth-order linear ordinary differential equation with four boundary conditions [24, 27]:

$$Y^{(4)} - \beta(1 - X)Y^{(2)} + \beta Y^{(1)} = \gamma, \quad 0 \leq X \leq 1, \quad (3)$$

$$Y(0) = Y^{(1)}(0) = Y^{(2)}(1) = Y^{(3)}(1) + \alpha_N \beta = 0, \quad (4)$$

where  $X \equiv x/L$ ,  $Y(X) \equiv y(x)/L$  and  $Y^{(n)} \equiv d^n Y(X)/dX^n$  for  $n = 0, 1, 2, \dots$ , respectively. The non-dimensional parameters  $\alpha_N$ ,  $\beta$  and  $\gamma$  are defined as

$$\alpha_N \equiv \frac{t_N}{L}, \quad \beta \equiv \frac{\sigma_t w L^3}{E^* I_N}, \quad \gamma \equiv \frac{\sigma_n w L^3}{E^* I_N}. \quad (5)$$

The value of  $\alpha_N$  is dependent on the surface loadings and is genuinely varying throughout the stressed beam, i.e.  $\alpha_N = \alpha_N(X)$ . For the sake of simplicity,  $\alpha_N$  is set as a constant and is considered as the average locus of the neutral surface in the following analysis. It is noted that since modelling equation (3) is linear and boundary conditions (4) are independent of  $\gamma$ , the homogeneous part of the solution of (3) is exactly the same as that of model # 3 in [21], which will be shown in the next subsection.

### 2.2. Derivation of the analytical solution

The analytical solution  $Y(X)$  to (3) and (4) is derived as follows [24]: integrating (3) in part with the boundary condition  $Y^{(3)}(1) + \alpha_N \beta = 0$  in (4) gives

$$Y^{(3)} - \beta(1 - X)(Y^{(1)} - \beta^{-1}\gamma) = -\alpha_N \beta. \quad (6)$$

Let

$$Z(X) \equiv Y^{(1)}(X) - \beta^{-1}\gamma. \quad (7)$$

Rewrite (6) and (4) as

$$Z^{(2)} - \beta(1 - X)Z = -\alpha_N\beta, \quad (8)$$

$$Z(0) + \beta^{-1}\gamma = Z^{(1)}(1) = 0. \quad (9)$$

Note that (8) can be solved and presented in terms of Airy and Scorer's functions [24–26]:

$$Z(X) = c_A Ai(\lambda(1 - X)) + c_B Bi(\lambda(1 - X)) + c_G Gi(\lambda(1 - X)) \quad (10)$$

in which  $\lambda$  is a scaling factor,  $Ai(X)$  and  $Bi(X)$  are the first and second kinds of the Airy functions, respectively, and  $Gi(X)$  is Scorer's function defined as [25, 26]

$$Gi(x) = Ai(x) \int_0^x Bi(t) dt + Bi(x) \int_x^\infty Ai(t) dt. \quad (11)$$

The scaling factor  $\lambda$  and the coefficient  $c_G$  are determined by substituting (10) and (11) into (8), which give

$$\lambda = \beta^{1/3}, \quad c_G = \pi\alpha_N\beta\lambda^{-2}. \quad (12)$$

From boundary conditions (9), the coefficients  $c_A$  and  $c_B$  are solved and presented in association with  $c_G$  in matrix form as

$$\mathbf{c} = \mathbf{A}^{-1} \cdot \mathbf{u} \quad (13)$$

in which

$$\mathbf{c} = [c_A \quad c_B \quad c_G]^T, \quad \mathbf{u} = \left[ -\frac{\gamma}{\beta} \quad 0 \quad \frac{\pi\alpha_N\beta}{\lambda^2} \right]^T, \quad (14)$$

$$\mathbf{A} = \begin{bmatrix} Ai(\lambda) & Bi(\lambda) & Gi(\lambda) \\ Ai^{(1)}(0) & Bi^{(1)}(0) & Gi^{(1)}(0) \\ 0 & 0 & 1 \end{bmatrix}.$$

The analytical solutions for the deflection and curvature of the stressed cantilever are calculated from (7), (10) and (11), with the coefficients  $c_A$ ,  $c_B$  and  $c_G$  evaluated by (13) and (14), as

$$Y(X) = \int_0^X [Z(\xi) + (\beta^{-1}\gamma)] d\xi = \frac{c_A}{\lambda} \int_{\lambda\eta}^\lambda Ai(\xi) d\xi + \frac{c_B}{\lambda} \int_{\lambda\eta}^\lambda Bi(\xi) d\xi + \frac{c_G}{\lambda} \int_{\lambda\eta}^\lambda Gi(\xi) d\xi + \left(\frac{\gamma}{\beta}\right) X, \quad (15)$$

$$Y^{(2)}(X) = Z^{(1)}(X) = -\lambda[c_A Ai^{(1)}(\lambda\eta) + c_B Bi^{(1)}(\lambda\eta) + c_G Gi^{(1)}(\lambda\eta)]$$

in which  $\eta = 1 - X$ .

### 2.3. Remarks

The deflection profile can also be solved by the series solution method [27], by which  $Y(X)$  is presented as a convergent infinite polynomial [28–30] in terms of the loading scenario. Details of the coefficients of the series solution are given in appendix A.

From (10)–(15), the deflection  $Y(X)$  can be decomposed as

$$Y(X) = \alpha_N Y_{\alpha_N}(X) + \gamma Y_\gamma(X). \quad (16)$$

Both the reduced deflection components,  $Y_{\alpha_N}(X)$  and  $Y_\gamma(X)$ , are functions of  $X$  and  $\beta$ , respectively. The linear dependence of  $Y(X)$  on  $\alpha_N$  and  $\gamma$  is also manifested from the series solution (A.2)–(A.4). It is noted that by setting  $\gamma = 0$ , the inhomogeneity of the present model disappears and the resultant homogeneous modelling equation and the solution  $Y_H(X)$  are identical to model #3 proposed by Zhang *et al* and the corresponding solution  $Y_Z(X)$  [21, 24, 27]:

$$Y_Z(X) \equiv Y_H(X) = \alpha_N Y_{\alpha_N}(X).$$

Hence, Zhang's model can be considered as a special case of the present model by discarding the surface loading in the normal direction.

## 3. Discussions

The most distinctive feature of the present model developed in section 2 is that the tangential and normal surface stresses are considered, by which the resultant deflection profile can be complicated and contain an inflection point due to the restoring bending moment contributed by the surface loadings in different directions. Meanwhile, for most of the cantilever-based devices the tip deflection is measured to evaluate the loading scenario for the designated applications. Nonetheless, such a measurement may fail the designated purpose since different loading scenarios can bend the cantilever with different deflection profiles albeit with the same tip deflection. In this section, the critical loading scenario and the inflection point for the deflection profile are investigated. The relationships of the tip deflection with different loading scenarios are analysed and demonstrated by numerical examples. A numerical algorithm is given in the appendix to solve the loading scenario by the analytical solution developed in section 2, by which the correct surface loadings can be formally determined for the designated applications of the cantilever-based devices.

### 3.1. The critical loadings for the deflection profile with inflection point

According to the fundamental theories of material mechanics and linear elasticity, the intrinsic bending moment can be represented by  $Y^{(2)}(X)$ , which can be obtained from (6) by

partial integration as

$$Y^{(2)}(X) = \alpha_N \beta (1 - X) + \frac{\gamma}{2} (1 - X)^2 + m(X), \quad (17)$$

$$m(X) = \beta (1 - X) Y(X) - \beta \int_X^1 Y(u) du.$$

For the cantilever characterized by the present model, the restoring bending moment inherent in (17) is admissible since the surface stresses in two directions are considered. In particular, due to the term  $m(X)$  in (17) it is conceivable that the resultant  $Y(X)$  is more complicated than that by the Stoney-type and other models [11, 21, 24]. In the meantime a cantilever experiences the curvature change as the direction of the intrinsic bending moment reverses at the critical point  $X_c$ ; that is,

$$Y^{(2)}(X_c) = 0. \quad (18)$$

The relationship of  $Y^{(2)}(X)$  and the loading scenario with  $\alpha_N \beta > 0$  is schematically demonstrated in figure 2(a), in which  $\alpha_N \beta$  represents the bending moment density contributed by the tangential surface stress. The contour  $Y^{(2)}(X) = 0$  separates the  $\gamma$ - $X$  plane into convex ( $Y^{(2)}(X) > 0$ ) and concave ( $Y^{(2)}(X) < 0$ ) regions, indicating that the direction of the intrinsic bending moment reverses at some critical location  $X_c$  along the cantilever when the normal surface stress  $\gamma$  is less than the critical  $\gamma_c$ , which can be evaluated by  $Y^{(2)}(0) = 0$  from (16) with given  $\alpha_N$  and  $\beta$  as

$$\gamma_c = -\alpha_N Y_{\alpha_N}^{(2)}(0) / Y_{\gamma}^{(2)}(0). \quad (19)$$

Figures 2(b) and (c) illustrate the deflection and curvature profiles at different normal surface stresses, in which  $\gamma_c = -0.413$  is evaluated by (19) with  $\alpha_N = 2.5 \times 10^{-2}$  and  $\beta = 10$ . The solid profiles are evaluated with  $\gamma = -0.813$ , along which the critical point  $X_c = 0.308$  is evaluated by (18) since  $\gamma \leq \gamma_c$ , as indicated by the circles in figures 2(b) and (c), respectively. The dashed profiles are evaluated with  $\gamma = -0.313$ , by which the entire cantilever is convexly bent since  $\gamma > \gamma_c$ , as illustrated by the convex region in figure 2(a). Hence, the deflection increases without being inflected since  $Y(0) = Y^{(1)}(0) = 0$  and  $Y^{(2)}(X) > 0$  for  $0 \leq X \leq 1$ .

The aforementioned description also applies when  $\alpha_N \beta < 0$ , with all the corresponding directions of the intrinsic bending moment reversed associated with  $\gamma \geq \gamma_c$  and  $\gamma < \gamma_c$ , as shown in figure 3(a). The solid profiles demonstrated in figures 3(b) and (c) are evaluated with  $\alpha_N = 2.5 \times 10^{-2}$ ,  $\beta = -1$  and  $\gamma = 8.13 \times 10^{-2}$ ; the corresponding critical value and the critical point are  $\gamma_c = 5.13 \times 10^{-2}$  and  $X_c = 0.403$ , respectively. The dashed profiles in figures 3(b) and (c) represent the non-inflected deflection and curvature evaluated by the same  $\alpha_N$  and  $\beta$  with  $\gamma = 5.03 \times 10^{-2}$ , respectively.

Two cases should be considered as  $\alpha_N \beta \approx 0$ : first, as manifested from (16) and (19):

$$\lim_{\alpha_N \rightarrow 0} Y(X) = \gamma Y_{\gamma}(X),$$

$$\lim_{\alpha_N \rightarrow 0} \gamma_c = 0.$$

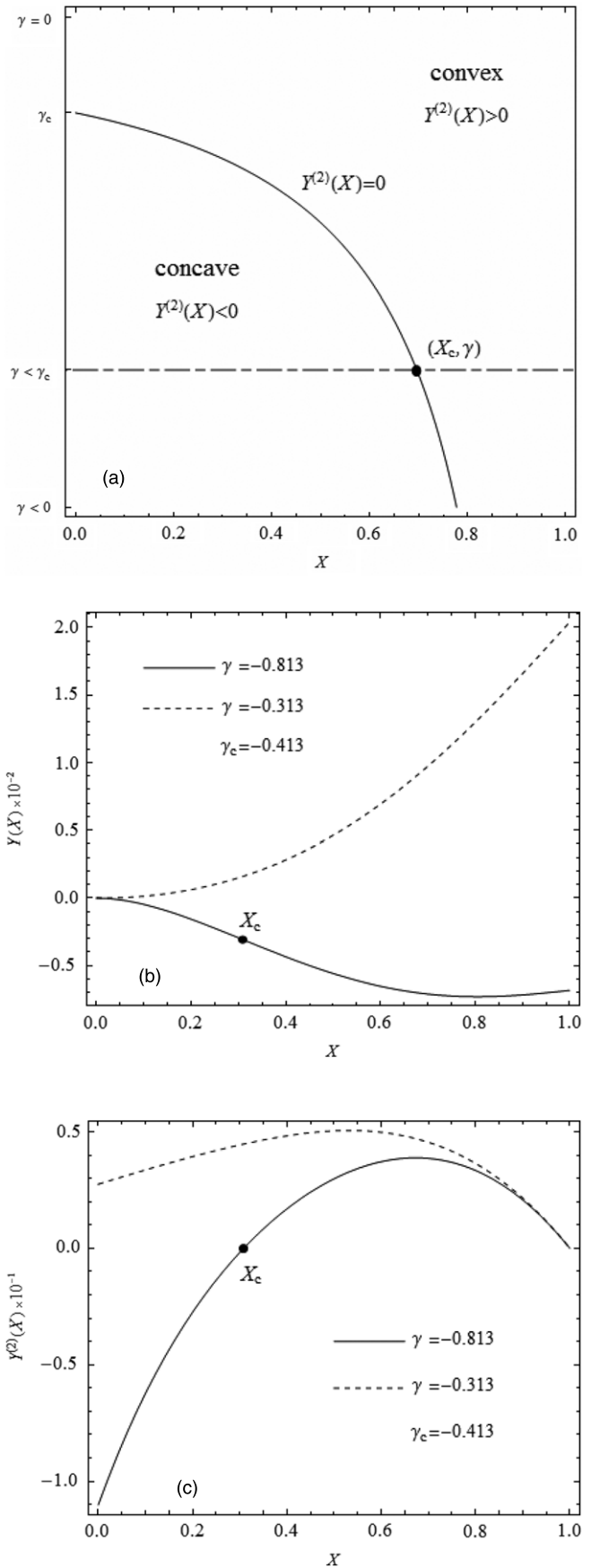
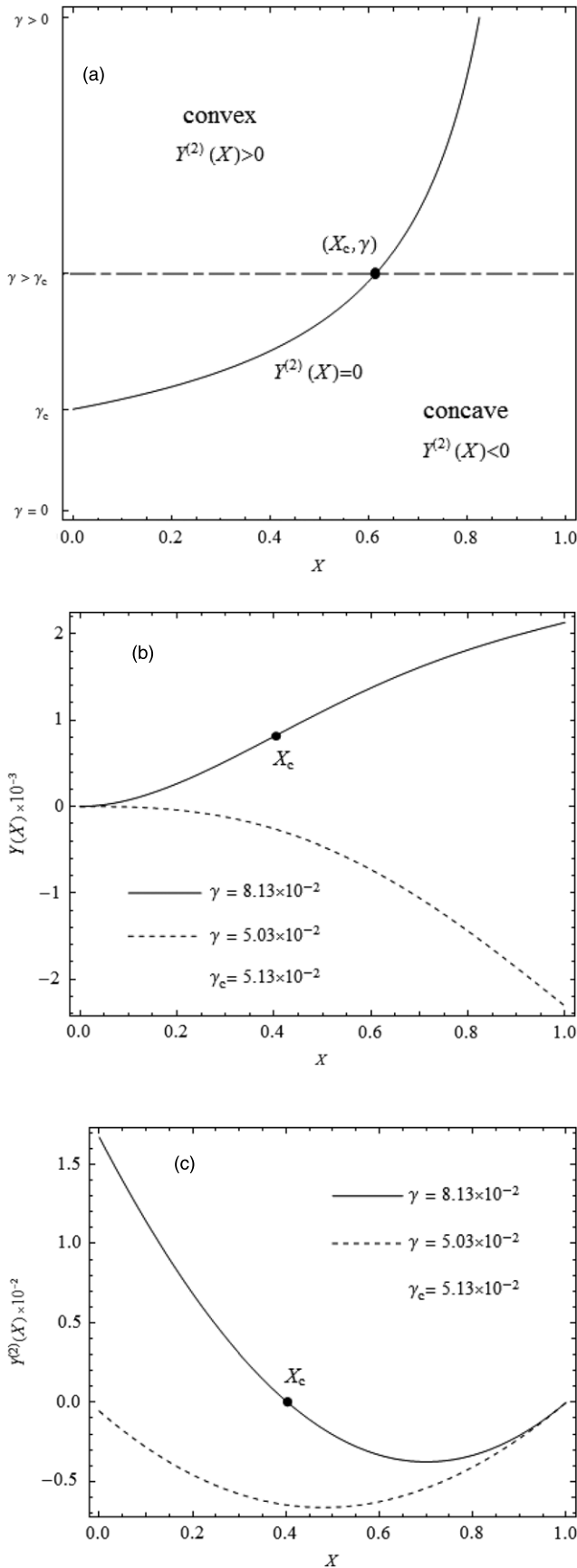


Figure 2. Relationships of the deflection, the intrinsic bending moment distribution and the loading scenario. (a)  $\alpha_N \beta > 0$ . (b) Deflection. (c) Intrinsic bending moment distribution ( $\alpha_N = 2.5 \times 10^{-2}$ ,  $\beta = 10$ ,  $\gamma_c = -0.413$ ,  $X_c = 0.308$ ).



**Figure 3.** Relations of the deflection, the intrinsic bending moment distribution and the loading scenario. (a)  $\alpha_N \beta < 0$ . (b) deflection. (c) Intrinsic bending moment distribution ( $\alpha_N = 2.5 \times 10^{-2}$ ,  $\beta = -1$ ,  $\gamma_c = 5.13 \times 10^{-2}$ ,  $X_c = 0.403$ ).

The cantilever is bent without being inflected since  $Y^{(2)}(X) \neq 0$  for  $0 \leq X < 1$  when  $\gamma \neq \gamma_c$ , as demonstrated in figures 4(a)–(c). The second case is that when  $\beta \equiv 0$ , modelling equations (3) and (4) become the Euler–Bernoulli beam equation loaded with a uniformly distributed normal surface stress, which can be solved as

$$Y(X) = \frac{\gamma}{24} X^2 (6 - 4X + X^2) \quad \text{if } \beta = 0.$$

This deflection profile is monotonic without inflection for arbitrary normal surface stress  $\gamma$  since  $Y^{(2)}(X) = \frac{\gamma}{2}(1 - X)^2$ . Finally, the tip of the cantilever is the trivial critical point regardless of the loading scenario since the boundary condition  $Y^{(2)}(1) = 0$  in (4), as demonstrated in figures 2(c), 3(c) and 4(c), respectively.

### 3.2. The relationship of the tip deflection and the surface loadings

Figures 5(a) and 6(a) demonstrate the relationship of the tip deflection and the loading scenario, in which the solid, dashed and dashed–dotted contours represent the same tip deflection evaluated at different normal surface stresses:  $\gamma < 0$ ,  $\gamma = 0$  and  $\gamma > 0$ , respectively. The points A, B and C in figure 5(a) are evaluated with  $\beta > 0$ , while P, Q and R in figure 6(a) are evaluated with  $\beta < 0$ , indicating that the depth of the neutral surface can be lifted up or lowered down, depending on the magnitudes and directions of the surface stresses. It is also manifested from (16) that  $\alpha_N$  is linearly dependent on  $\gamma$  at the same  $Y(1)$  and  $\beta$ . The deflection profiles of the same tip deflection by different loading scenarios are demonstrated in figure 5(b), in which the tip deflection  $Y(1) = 2 \times 10^{-2}$ , bent by  $\beta = 1$  with  $(\gamma, \alpha_N) = (-2.5, 1.002)$ ,  $(0, 6.748 \times 10^{-2})$  and  $(2.5, -0.867)$  for the solid, dashed and dashed–dotted profiles, respectively. The tip deflection in figure 6(b) is  $Y(1) = -2.25 \times 10^{-2}$ , bent by  $\beta = -1$  with  $(\gamma, \alpha_N) = (-2.5, -0.882)$ ,  $(0, 5.904 \times 10^{-2})$  and  $(2.5, 1)$ , as depicted by the solid, dashed and dashed–dotted profiles, respectively.

All the contours and deflection profiles shown in figures 5 and 6 reveal that the designated purpose of the cantilever-based device may fail by measuring the tip deflection to resolve the surface loadings, since the same tip deflection can be achieved by different loading scenarios. In fact, the quality and quantity of the experimental measurement depend on the parameters of the mechanical model employed to characterize the cantilever deflection. Therefore, two more measurements in addition to the tip deflection are required to determine the loading scenario, since the present model characterizes the deflection with three parameters:  $\beta$ ,  $\gamma$  and  $\alpha_N$ . In appendix B, a numerical algorithm is proposed that by assuming that the whole deflection profile is measurable, the loading scenario can be formally determined with the analytical solution developed in section 2 by the deflections measured at three arbitrarily selected locations along the cantilever.

## 4. Conclusion

By taking the tangential and the normal surface stresses into consideration, the present model exhibits its conformity to

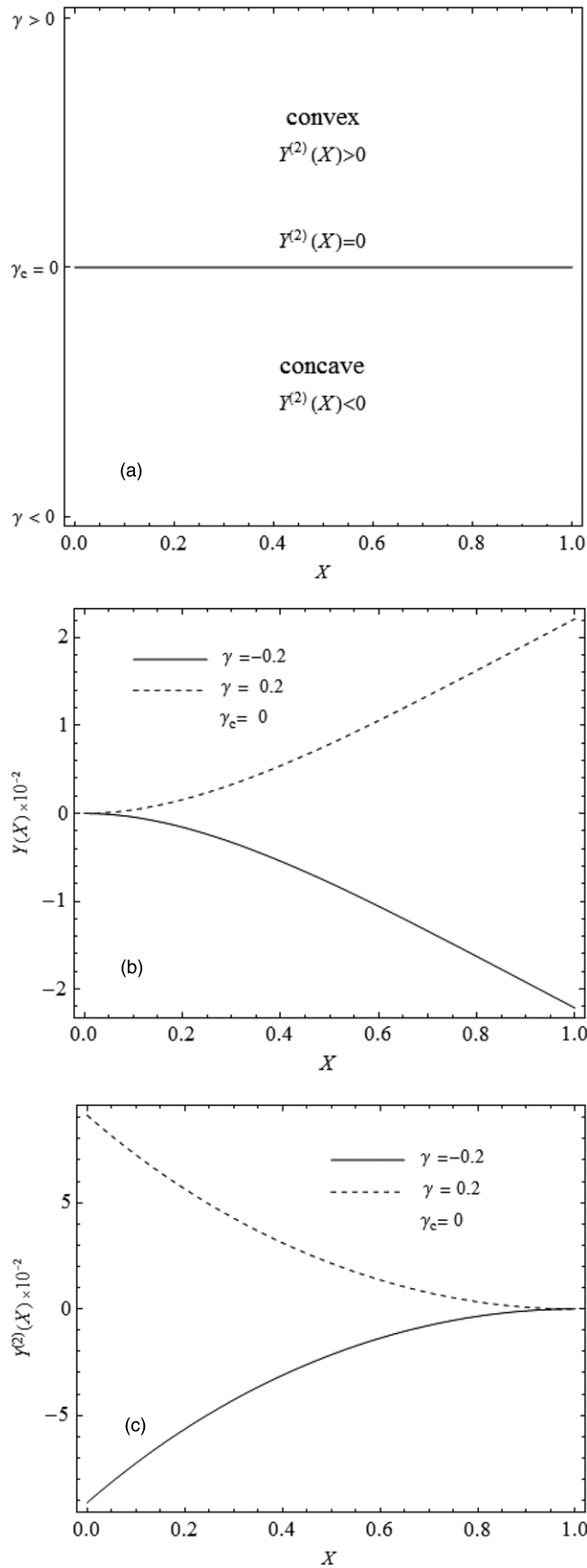


**Figure 4.** Relationships of the deflection, the intrinsic bending moment distribution and the loading scenario. (a)  $\alpha_N = 0$ . (b) Deflection. (c) Intrinsic bending moment distribution ( $\alpha_N = 0$ ,  $\beta = 1$ ,  $\gamma_c = 0$ ).

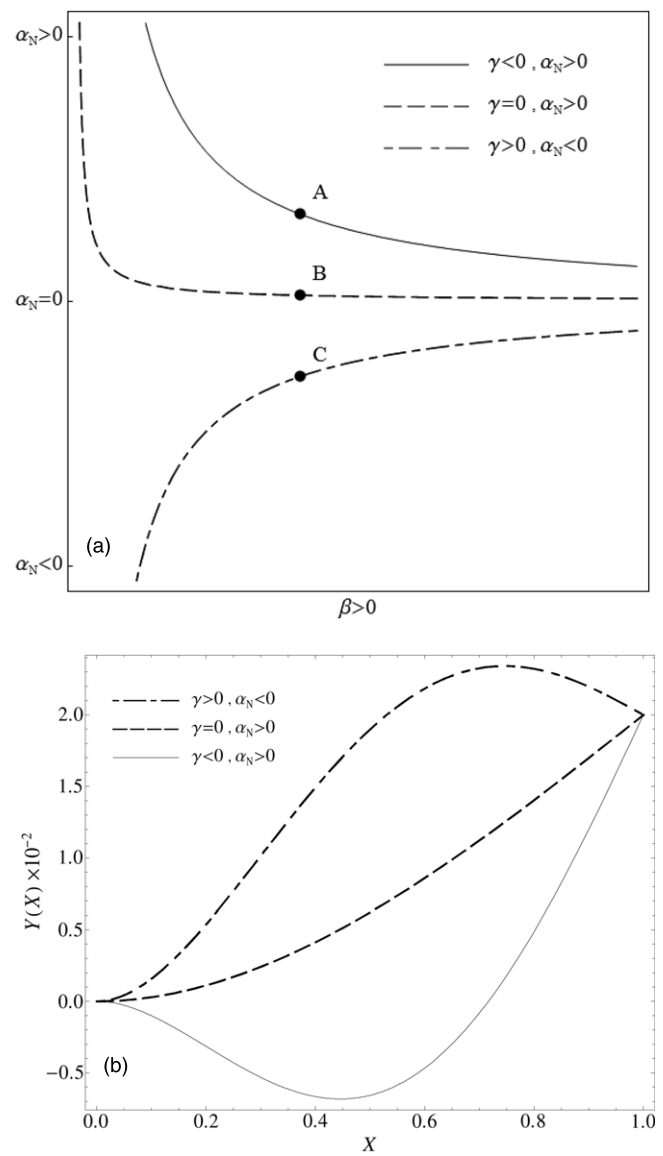


**Figure 5.** Relationships of the tip deflection and the loading scenario. (a) Contours of the same tip deflection with  $\beta > 0$ . (b) Deflection profiles of the same tip deflection by different loading scenarios.

the physical situation for the cantilever-based devices. The modelling equation and the numerical examples manifest that the present model comprises its predecessor proposed by Zhang *et al* as a special case by discarding the normal surface stress. The conditions for the critical surface loadings are developed from the analytical solution of the modelling equation, by which the restoring bending moment deflects the cantilever with one inflection point contained in the resultant deflection profile. The analysis of the relationship for the tip deflection and the loading scenario reveals the insufficiency of determining the loading scenario from the tip deflection. Since either the present, or the Stoney-type models adopting distributed surface loadings characterize the cantilever deflection with more than one parameters various loading scenarios can result in the different deflection profiles albeit with the same tip deflection. The authors suggest

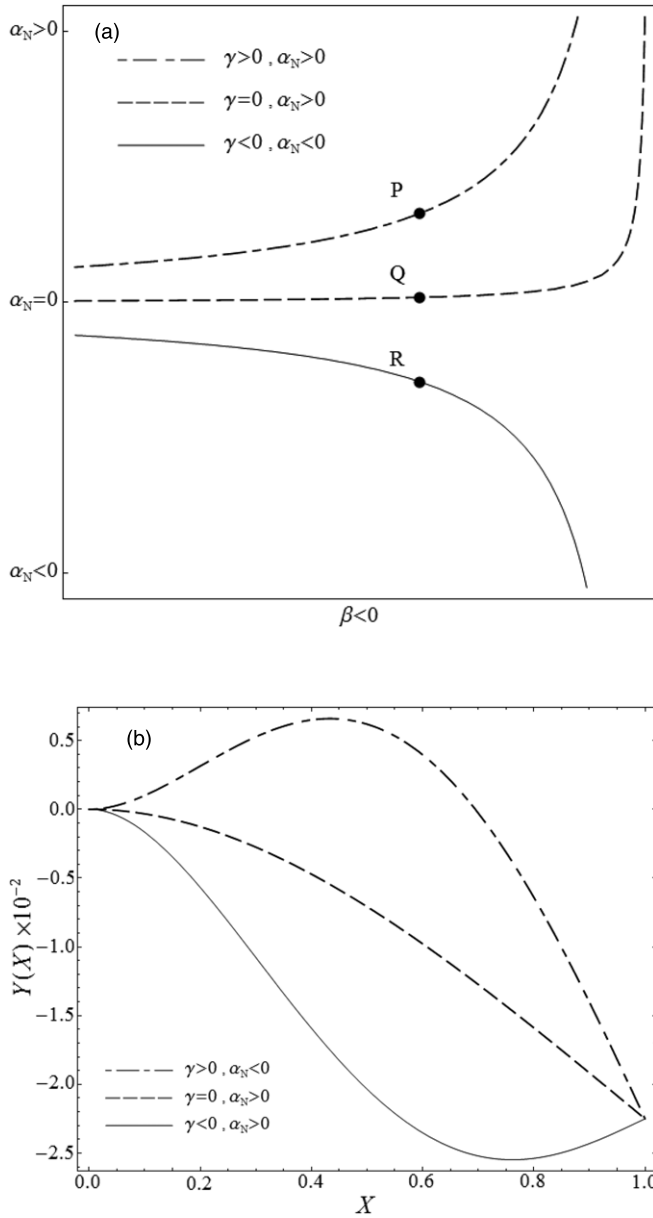


**Figure 6.** Relationships of the tip deflection and the loading scenario. (a) Contours of the same tip deflection with  $\beta < 0$ . (b) Deflection profiles of the same tip deflection by different loading scenarios.

that the whole deflection profile should be measured by any experimental methodology to determine the loading scenario with the proposed algorithm for the devices utilizing the cantilever structure.

### Appendix A.

The series solution for the deflection profile can be presented as [27–30]

$$Y(X) = \sum_{n=0}^{\infty} a_n X^{n+2} = Y_H(X) + Y_P(X), \quad 0 \leq X \leq 1 \quad (\text{A.1})$$

in which

$$a_n = (a_n)_H + (a_n)_P,$$

$$Y_H(X) = \sum_{n=0}^{\infty} (a_n)_H X^{n+2}, \quad (\text{A.2})$$

$$Y_P(X) = \sum_{n=0}^{\infty} (a_n)_P X^{n+2}.$$

The coefficients  $(a_n)_H$  and  $(a_n)_P$  can be presented in terms of  $\alpha$ ,  $\beta$  and  $\gamma$  as

$$(a_0)_H = \frac{\alpha_N \beta}{2} \frac{\sum_{n=0}^{\infty} \frac{\beta^n}{(3n+1)!} \prod_{k=0}^{n-1} (3k+1)}{1 + \sum_{n=0}^{\infty} \beta^{n+1} \frac{3n+1}{(3n+3)!} \prod_{k=0}^{n-1} (3k+1)},$$

$$(a_1)_H = -\frac{\alpha_N \beta}{6}, \quad (a_2)_H = \frac{\beta}{12} (a_0)_H, \quad (\text{A.3})$$

$$(a_{n+3})_H = \beta \frac{(n+3)!}{(n+5)!} \times \left[ (a_{n+1})_H - \frac{n+2}{n+3} (a_n)_H \right],$$

$$n = 0, 1, 2, \dots,$$

and

$$(a_0)_P = \frac{\gamma}{2} \frac{\sum_{n=0}^{\infty} \frac{3n+1}{3n+2} \times \frac{\beta^n}{(3n+1)!} \prod_{k=0}^{n-1} (3k+1)}{1 + \sum_{n=0}^{\infty} \beta^{n+1} \frac{3n+1}{(3n+3)!} \prod_{k=0}^{n-1} (3k+1)},$$

$$(a_1)_P = -\frac{\gamma}{6}, \quad (a_2)_P = \frac{\gamma}{24} + \frac{\beta}{12} (a_0)_P, \quad (\text{A.4})$$

$$(a_{n+3})_P = \beta \frac{(n+3)!}{(n+5)!} \times \left[ (a_{n+1})_P - \frac{n+2}{n+3} (a_n)_P \right],$$

$$n = 0, 1, 2, \dots,$$

where

$$\prod_{k=m}^n f_k \equiv \begin{cases} f_m \times f_{m+1} \times \dots \times f_n & \text{if } n > m, \\ 1 & \text{otherwise,} \end{cases} \quad (\text{A.5})$$

Note that  $0^0 \equiv 1$  and  $0^n \equiv 0$  if  $n \neq 0$  in (A.3) and (A.4). Details of the derivations of (A.3) and (A.4) and the related mathematical properties can be referred to in [27–30].

### Appendix B.

As mentioned in section 3.2, the cantilever-based device may fail the designated purpose by measuring the loading scenario from the tip deflection, since the same tip deflection can be achieved by various loading scenarios. In this appendix, a numerical algorithm is proposed to formally determine the loading scenario characterized by the present model.

Suppose that the whole deflection profile is measurable; so three locations  $\tilde{X}_1$ ,  $\tilde{X}_2$  and  $\tilde{X}_3$  along the cantilever can be

selected at one's disposal, at which the measured deflections are denoted as  $\tilde{Y}_1$ ,  $\tilde{Y}_2$  and  $\tilde{Y}_3$ , respectively. Note that the fixed end,  $\tilde{X} = 0$ , should be excluded since  $Y(\tilde{X}) = 0$  is trivial by boundary condition (4). From (16),  $\tilde{Y}_1$  can be presented as

$$\tilde{Y}_1 = \alpha_N Y_{\alpha_N}(\tilde{X}_1) + \gamma Y_\gamma(\tilde{X}_1). \quad (\text{B.1})$$

Since  $Y(X)$  is linearly dependent on  $\alpha_N$  and  $\gamma$ , they can be solved and presented in matrix form in terms of the other measured quantities as

$$\begin{bmatrix} \alpha_N \\ \gamma \end{bmatrix} = \begin{bmatrix} Y_{\alpha_N}(\tilde{X}_2) & Y_\gamma(\tilde{X}_2) \\ Y_{\alpha_N}(\tilde{X}_3) & Y_\gamma(\tilde{X}_3) \end{bmatrix}^{-1} \cdot \begin{bmatrix} \tilde{Y}_2 \\ \tilde{Y}_3 \end{bmatrix}. \quad (\text{B.2})$$

Obviously,  $\alpha_N$  and  $\gamma$  in (B.2) are functions of  $\beta$  only, since both the reduced deflections  $Y_{\alpha_N}(X)$  and  $Y_\gamma(X)$  are functions of  $X$  and  $\beta$ , respectively. Hence, the value of  $\beta$  can be solved by substituting (B.2) into (B.1), from which the result can be presented as

$$\begin{aligned} \beta &= \beta(\tilde{X}_1, \tilde{X}_2, \tilde{X}_3), \\ \tilde{\mathbf{X}}_k &\equiv (\tilde{X}_k, \tilde{Y}_k), \quad k = 1, 2, 3. \end{aligned} \quad (\text{B.3})$$

The values of  $\alpha_N$  and  $\gamma$  can be solved from (B.2) with (B.3), which can be presented as

$$\begin{aligned} \alpha_N &= \alpha_N(\tilde{X}_1, \tilde{X}_2, \tilde{X}_3), \\ \gamma &= \gamma(\tilde{X}_1, \tilde{X}_2, \tilde{X}_3). \end{aligned} \quad (\text{B.4})$$

As shown in (B.3) and (B.4), the loading scenario is formally solved by the deflections measured at three arbitrarily selected locations along the cantilever.

*Special case.* When the critical point  $\tilde{X}_c$  is detected within the cantilever, as mentioned in section 3.1, the proposed algorithm can be simplified as follows. Let the deflections  $\tilde{Y}_1$  and  $\tilde{Y}_c$  be measured at  $\tilde{X}_1$  and  $\tilde{X}_c$ , respectively. From (B.2)

$$\begin{bmatrix} \alpha_N \\ \gamma \end{bmatrix} = \begin{bmatrix} Y_{\alpha_N}(\tilde{X}_1) & Y_\gamma(\tilde{X}_1) \\ Y_{\alpha_N}(\tilde{X}_c) & Y_\gamma(\tilde{X}_c) \end{bmatrix}^{-1} \cdot \begin{bmatrix} \tilde{Y}_1 \\ \tilde{Y}_c \end{bmatrix}. \quad (\text{B.5})$$

On the other hand,  $Y^{(2)}(\tilde{X}_c) = \alpha_N Y_{\alpha_N}^{(2)}(\tilde{X}_c) + \gamma Y_\gamma^{(2)}(\tilde{X}_c) = 0$  since  $\tilde{X}_c$  is the critical point, from which

$$\frac{\gamma}{\alpha_N} = -\frac{Y_{\alpha_N}^{(2)}(\tilde{X}_c)}{Y_\gamma^{(2)}(\tilde{X}_c)}. \quad (\text{B.6})$$

The loading scenario can be formally solved from (B.5) and (B.6), which can be presented as

$$\begin{aligned} \alpha_N &= \alpha_N(\tilde{\mathbf{X}}_1, \tilde{\mathbf{X}}_c), \\ \beta &= \beta(\tilde{\mathbf{X}}_1, \tilde{\mathbf{X}}_c), \\ \gamma &= \gamma(\tilde{\mathbf{X}}_1, \tilde{\mathbf{X}}_c). \end{aligned} \quad (\text{B.7})$$

## References

- [1] Sandeep K V 2007 *AZojono: J. Nanotechnol. Online* doi:10.2240/azojono0115 (<http://www.azonano.com/Details.asp?ArticleID=1927>)
- [2] Whitesides G M 1995 *Sci. Am.* **273** 146–9
- [3] Fritz J et al 2000 *Sci. New Ser.* **288** 316–8
- [4] Wu G et al 2001 *Proc. Natl Acad. Sci. USA* **98** 1560–4
- [5] Alvarez M et al 2003 *Biosens. Bioelectron.* **18** 649–53
- [6] Shu W, Laue E D and Seshia A A 2006 *Biosens. Bioelectron.* **22** 2003–9 (PMID: 17045792)
- [7] Ibach H 1997 *Surf. Sci. Rep.* **29** 193–263
- [8] Berger R et al 1997 *Science* **276** 2021–4
- [9] Lin S et al 2005 *Curr. Proteomics* **2** 55–81
- [10] Hagan M F et al 2002 *J. Phys. Chem. B* **106** 10163–73
- [11] Stoney G G 1909 *Proc. R. Soc. Lond. Ser. A* **82** 172–5
- [12] Vilms J and Kerps D 1982 *J. Appl. Phys.* **53** 1536–7
- [13] Townsend P H, Barnett D M and Burner T A 1987 *J. Appl. Phys.* **62** 4438–44
- [14] Freund L B, Floro J A and Chason E 1999 *Appl. Phys. Lett.* **74** 1987–9
- [15] Klein C A 2000 *J. Appl. Phys.* **88** 5487–9
- [16] Godin M et al 2001 *Appl. Phys. Lett.* **79** 551–3
- [17] Sader J E 2001 *J. Appl. Phys.* **89** 2911–21
- [18] Hsueh C H, Lee S and Chung T J 2003 *J. Appl. Mech.* **70** 151–4
- [19] Nikishkov G P 2003 *J. Appl. Phys.* **94** 5333–6
- [20] Hu Y Y and Huang W M 2004 *J. Appl. Phys.* **96** 4154–60
- [21] Zhang Y et al 2004 *J. Phys. D: Appl. Phys.* **37** 2140–5
- [22] Landau L D and Lifshitz E M 1975 *Theory of Elasticity* 2nd edn (Oxford: Pergamon)
- [23] Gere J M 2004 *Mechanics of Materials* (Belmont, CA: Brooks/Cole-Thomson Learning)
- [24] S-H Tsai and Kan H-C 2008 *J. Phys. D: Appl. Phys.* **41** 095502
- [25] Abramowitz M and Stegun I A (ed) 1972 *Handbook of Mathematical Functions with Formulas, Graphs, and Mathematical Tables* 9th printing (New York: Dover)
- [26] Lebedev N N 1972 *Special Functions and Their Applications* (New York: Dover)
- [27] Tsai S-H and Kan H-C 2007 *J. Phys. D: Appl. Phys.* **40** 6129–37
- [28] Apostol T M c1974 *Mathematical Analysis* 2nd edn (Reading, MA: Addison-Wesley)
- [29] Grossman S I and Derrick W R 1988 *Advanced Engineering Mathematics* (New York: Harper and Row)
- [30] Birkhoff G and Rota G C 1989 *Ordinary Differential Equations* 4th edn (New York: Wiley)